Organic & Biomolecular Chemistry

Dynamic Article Links

Cite this: *Org. Biomol. Chem.*, 2011, **9**, 8268

www.rsc.org/obc

PAPER

Tautomerism in Schiff bases. The cases of 2-hydroxy-1-naphthaldehyde and 1-hydroxy-2-naphthaldehyde investigated in solution and the solid state†

R. Fernando Martínez,*[a] Martín Ávalos,[a] Reyes Babiano,[a] Pedro Cintas,[a] José L. Jiménez,[a] Mark E. Light[b] and Juan C. Palacios[a]

Received 3rd July 2011, Accepted 5th September 2011
DOI: 10.1039/c1ob06073b

Schiff bases derived from hydroxyl naphthaldehydes and *o*-substituted anilines have been prepared and their tautomerism assessed by spectroscopic, crystallographic, and computational methods. Tautomeric equilibria have also been studied and reveal in most cases a slight preference of imine tautomers in solution; a fact supported by DFT calculations in the gas phase as well as incorporating solvent effects through the SMD model. To simulate the effect exerted by the crystal lattice on tautomer stability, we have developed a computational protocol in the case of 1-*tert*-butyl-2-(2-hydroxy-1-naphthylmethylene)aminobenzene whose data have been obtained experimentally at 120 K. Although a rapid imine-enamine interconversion may be occurring in the solid state, the imine tautomer becomes the most stable form and the energy difference should be related to the difference in the packing of the molecules.

Introduction

Schiff bases derived from *o*-hydroxybenzaldehyde (salicylaldehyde) have attracted a great interest not only for their biological and photophysical properties (thermo- and photochromism, and non-linear optical behavior),[1] but also as model compounds for assessing the nature of the hydrogen bonding.[2] In this context and due to intramolecular hydrogen bonding, Schiff bases from 2-hydroxy-1-naphthaldehyde can exhibit phenolimine-ketoenamine (or zwitterionic) tautomeric structures (**1–3**) both in solution[3] and the crystalline state.[4]

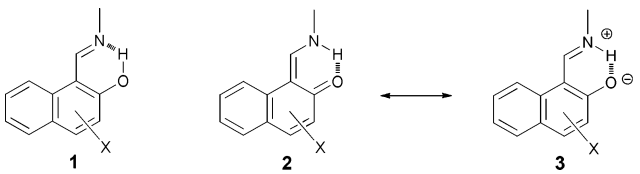

1 **2** **3**

However, most crystal data for Schiff bases derived from 2-hydroxy-1-naphthaldehyde and arylamines (**4**,[5a] **5**,[5b] **6**,[5c] **7**,[5d] **8**,[5e] **9**,[5f] **10**[5g]), alkylamines (**11**,[6] **12**[6]), and heterocyclic amines (**13**,[7] **14**[8]) are consistent with enamine tautomers, even though one benzene ring loses its aromatic character.

Moreover, a further re-investigation on the structure of the adduct arising from 2-hydroxy-1-naphthaldehyde and n-propylamine, which was previously described as imine,[9] shows to be enamine.[10] An intriguing case is exemplified by **15** because both tautomers co-exist in the same structure,[11] while there are two molecules with different structure, imine (**16**) and enamine (**17**), in the unit cell of the Schiff base derived from 2-aminopyridine at room temperature.[12] Several Schiff bases with zwitterionic structures have been reported as well (**18**,[13] **19**,[14] **20**[15]). Most of the less common zwitterionic structures come from aliphatic amines.[16]

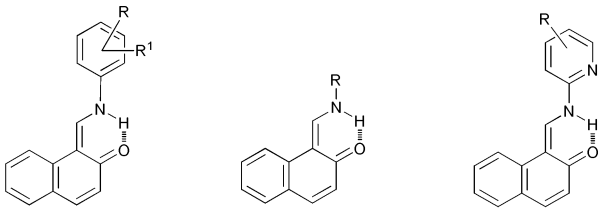

4 R = 3-CO_2H, R^1 = H
5 R = 4-$COCH_3$, R^1 = H
6 R = 4-NO_2, R^1 = H
7 R = 4-OH, R^1 = H
8 R = 2-MeO, R^1 = H
9 R = 2-OH, R^1 = 5-Cl
10 R = 2-OH, R^1 = 5-Me

11 R = 1-adamantyl
12 R = 2-adamantyl

13 R = 4-Me
14 R = 3-OH

These compounds show invariably an enamine structure in solution. For example, the Schiff base from 2-hydroxy-1-naphthaldehyde and 3-chloroaniline is an enamine tautomer in DMSO-d_6 solution, though it is imine in the solid state at 200 K.[17] Spectroscopic data also point to enamine structures for the condensation products derived from 1,4-diformyl-2,3-dihydroxynaphthalene in solution[18] (**21, 22**) and, likewise X-ray diffractometry confirms the dienamine structure for both in the solid state at −100 °C. Similarly, the macrocycle **23**, generated

[a]*Departamento de Química Orgánica e Inorgánica, QUOREX Research Group, Facultad de Ciencias-UEX, E-06006, Badajoz, Spain. E-mail: rmarvaz@unex.es*
[b]*Department of Chemistry, The University of Southampton, Highfield, Southampton, U.K, SO17 1BJ*

† Electronic supplementary information (ESI) available: Figures S1–S3, Tables S1–S6, and computational data. CCDC reference numbers 805572–805574 and 810937. For ESI and crystallographic data in CIF or other electronic format see DOI: 10.1039/c1ob06073b

by condensation of an *ortho*-phenylendiamine derivative, shows sixfold enaminone tautomers.[18]

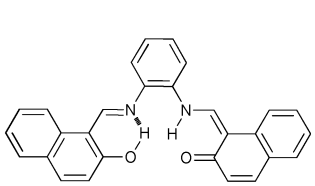

15

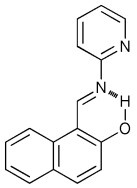

16

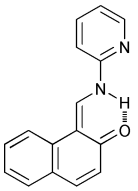

17

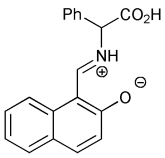

18

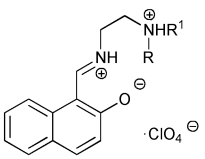

19 R = R^1 = Me
20 R = H, R^1 = CH_2CH_2OH

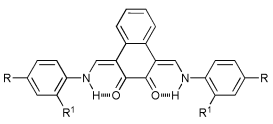

21 R = MeO, R^1 = H
22 R = H, R^1 = NH^tBoc

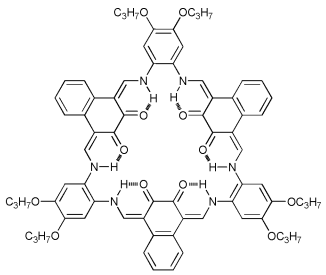

23

Motivated by the above-mentioned results and the comprehensive literature of Schiff bases tautomerism, often reporting contradictory data, we recently embarked on the structural elucidation of Schiff bases derived from tris(hydroxymethyl)aminomethane, usually abbreviated as TRIS,[19,20] and found an enamine structure for **24** in both the solid state and solution. Herein, we extend this study to Schiff bases generated from 2-hydroxy-1-naphthaldehyde and 1-hydroxy-2-naphthaldehyde and some *ortho*-substituted anilines. These amines were chosen in the hope that the steric effects will disrupt the coplanar arrangement between the imine bond and the aromatic ring, thereby enabling the delocalization of the nitrogen lone pair through the latter ring. As a result both the availability of the lone pair, and hence the basicity, would decrease, thus inhibiting hydrogen transfer from the phenol group and favoring an imine structure both in solution and the solid state.

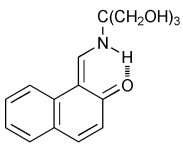

24

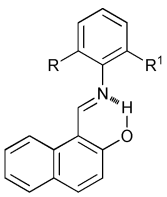

25 R = H, R^1 = ^{t}Bu
26 R = R^1 = Me

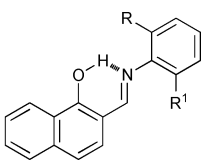

27 R = H, R^1 = ^{t}Bu
28 R = R^1 = Me

Since equilibria between enamine and imine tautomers have been observed for **25–28** in the crystal lattice (measured at 120 K) and in solution, this behavior has further been explored through computational calculations at B3LYP/6-31G** and M06-2X/6-311++G** levels.[21]

Results and discussion

Syntheses and solid-state structures

The experimental protocol involves the condensation of equimolar amounts of 2-hydroxy-1-naphthaldehyde (or 1-hydroxy-2-naphthaldehyde) with 2-*tert*-butylaniline and 2,6-dimethylaniline in ethanol at room temperature. The resulting Schiff bases **25–28** could thus be obtained in a few minutes with moderate to good yields (72–88%), although such syntheses were not optimized.

Predictions about solid-state structures are quite difficult without the assistance of X-ray diffraction data. IR spectroscopy for instance does not enable a clear-cut assignment of imine or enamine structures, because the stretching vibrations for the C=N (imine) and C=O (enamine) bonds usually overlap.[22] However, the intensity of the latter is much stronger (it uses to be the most intense band of the spectrum) than that of the less polar C=N bond. Nevertheless, a comparison of IR intensities for structural elucidation should be taken with caution.

FT-IR spectra of compounds **25–28** are similar (Figure S1, ESI†). The most relevant absorption appears at ~1620 cm^{-1} in the case of 2-hydroxy-1-naphthaldehyde derivatives, while it is found at ~1605 cm^{-1} for those of 1-hydroxy-2-naphthaldehyde. This band, together with the presence of absorptions for the phenol C–O bond at ~1330 cm^{-1}, allowed us to conclude that compounds **25–28** most likely exhibit imine structures in the solid state at room temperature. As we shall see, this conclusion agrees with their X-ray diffraction analyses.

Thus, crystal data for compounds **25–28** recorded at 120 K are shown in Fig. 1.[23]

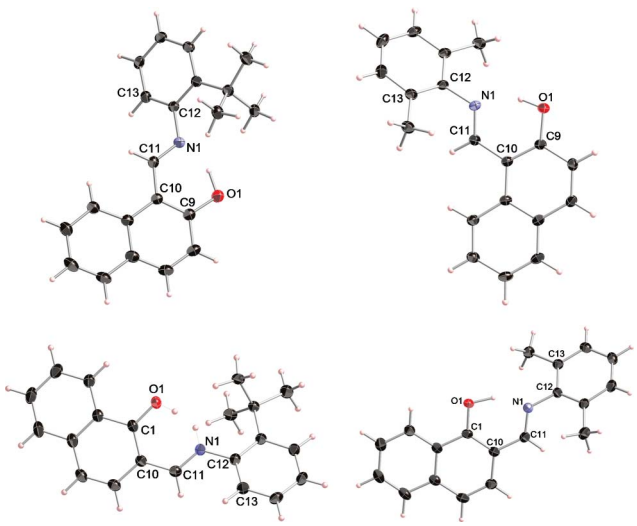

Fig. 1 X-Ray structure of **25–28** at 120 K (thermal ellipsoids drawn at the 35% probability level).

Tables S1–S4 (see ESI†) collect some bond lengths and bond angles for such compounds, which have been determined both experimentally and calculated at two DFT levels of theory and taken into account imine and enamine tautomers in each case (see later).

The assignment of imine structures for **25–28** in the solid state is supported by the following facts: long C–O bond lengths (1.355, 1.351, 1.315, and 1.337 Å, respectively) accompanied by short C=N bonds corresponding to an imine tautomer (1.291, 1.290,

1.305, and 1.289 Å, respectively), as well as the refined position of the hydrogen atom linked to the oxygen. Furthermore, the experimentally-measured C–O and C═N bond lengths match those calculated at both the B3LYP/6-31G** and M06-2X/6-311++G** levels (~1.33 and ~1.29 Å for C–O and C═N, respectively) (see later). However, the structure of **24** was found to be enamine in the solid state at 120 K,[20] as C–O and C═N bond lengths (1.283 and 1.313 Å, respectively) become shorter and larger than those in **25–28**.

The C–O and C═N bonds in **27** are significantly shorter and longer, respectively, than those of **25, 26**, and **28**. Such intermediate values are consistent with average values between the corresponding bond lengths in imine and enamine forms.

Fig. 2 shows the electron density difference Fourier maps for the four refinements without including the hydrogen in the model. These clearly show that the hydrogen atom is much localized on the oxygen in **25** and **26**, but in both cases there is a hint of some density towards the nitrogen. In the case of **27** and **28** the proton is rather delocalized between the two positions, *i.e.* the hydrogen partly bound to oxygen and nitrogen atoms. This suggests the co-existence of imine and enamine tautomers in a fast equilibrium within the crystal lattice.

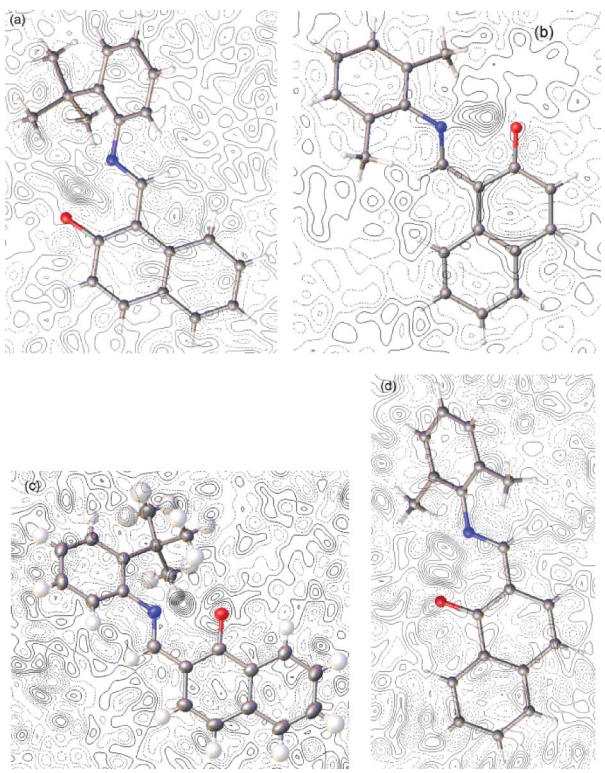

Fig. 2 Electron density difference maps for **25** (a), **26** (b), **27** (c), and **28** (d).

Since both tautomers contain a strong intermolecular hydrogen bond involving the iminic nitrogen and the vicinal OH group (N···H–O), the characteristic data of such bonds have been gathered in Table 1.

Remarkably, the steric hindrance caused by *ortho*-substitution at the aniline ring leads to the lack of coplanarity in the solid-state structures of **25–28**. Thus, the angles between aniline and naphthalene rings are close to 35–45° (44.43, 40.31, 36.35, and 46.80°, respectively); this value reflecting a balance situation because the orthogonal disposition between such rings would also minimize the electronic delocalization and steric effects.

Table 1 Hydrogen bonds [Å and °] for compounds **25–28**

Comp.	*D*–H···*A*	*d*(*D*–H)	*d*(H···*A*)	*d*(*D*···*A*)	∠(*DHA*)
25	O1–H1···N1	1.044	1.587	2.558(2)	152.2
26	O1–H1···N1	0.904	1.723	2.547(2)	150.2
27	O1–H1···N1	0.840	1.843	2.552(2)	141.0
	N1–H2···O1	0.880	1.847	2.552(2)	135.6
28	O1–H1···N1	1.071	1.569	2.556(2)	150.3

Structures in solution

An imine tautomer can easily be identified by the presence of two singlets in the ^{1}H NMR spectrum: one deshielded signal (~13–15 ppm) corresponding to the phenol proton bound intramolecularly, and the other attributed to the iminic proton (~8.5–9.5 ppm). On the other hand, an enamine structure shows two coupled doublets: one corresponding to the NH proton involved in the intramolecular bond as well, which is significantly deshielded (~14–16 ppm), and the ethylenic proton of enamine fragment (~8.5–10 ppm). Clearly the multiplicity of such signals is the key to distinguish them as chemical shifts are quite similar in both tautomers.[12,24,25] Like in the solid state, the structure in solution may be altered by temperature changes.[26,27] Table 2 collects some relevant NMR data for compounds **25–28** (Figure S2, see ESI†).

Significant differences between imine and enamine structures can instead be extracted from ^{13}C NMR spectra through diagnostic signals, because it has been reported that the phenol carbon of imines is usually more shielded than the corresponding carbonyl carbon of enamines (~160 ppm *versus* ~180 ppm).[25] This trend can also be detected in their ^{15}N NMR spectra as the iminic nitrogen is much more shielded than the nitrogen atom in enamines (~ −63 ppm *versus* ~ −247 ppm).[26,28–32]

However, the C-2 signal in **25–28**, which resonates between the phenol carbon of imines and the carbonyl signal of enamines (~168 ppm), together with small coupling constants ($J_{NH,H}$ = ~3–4 Hz) is evidence again of a rapid imine-enamine equilibrium in DMSO-d_6 solution at room temperature (Figure S3, see ESI†).

Tautomeric equilibria

As mentioned above, there is a fast equilibrium in solution between both tautomers. The tautomerization constant K_T, has been previously determined through ^{13}C shifts of the phenol carbon or ^{15}N resonances of the iminic nitrogen, as well as by means of coupling constants, namely ^{15}N–H, ^{13}C–^{13}C and ^{13}C–^{15}N values.[26,29,33,34]

Table 2 Selected spectroscopic data[a] for **25–28**

Compound	OH/NH	$J_{NH,H}$	N–C*H*	N–*C*H	C-2
25	15.34s	0.0	9.46s	159.0	166.5
26	15.29d	2.4	9.44d	163.5	167.0
27	14.78d	3.5	8.77d	161.4	167.1
28	14.67d	4.4	8.61d	165.5	168.5

[a] δ in ppm and J in Hz.

The chemical shifts observed experimentally (δ_{exp}) are an average of those of imine and enamine forms (δ_i and δ_e, respectively). Accordingly, $\delta_{exp} = n_i\delta_i + n_e\delta_e$, where n_i and n_e denote the molecular populations of imine and enamine structures, respectively (obviously, $n_i + n_e = 1$). The same reasoning applies to coupling constants, which can be represented by the equation: $J_{exp} = n_iJ_i + n_eJ_e$. These simple equations can therefore be used to estimate tautomeric populations, assuming that δ_i/δ_e and J_i/J_e values are known. Thus:

$$n_i = (\delta_e - \delta_{exp})/(\delta_e - \delta_i) \text{ and } n_e = (\delta_{exp} - \delta_i)/(\delta_e - \delta_i)$$

The tautomerization constant ($K_T = [\text{enamine}]/[\text{imine}] = n_e/n_i$) for imine-enamine equilibria may then be expressed by:

$$K_T = n_e/n_i = (\delta_{exp} - \delta_i)/(\delta_e - \delta_{exp}) = (J_{exp} - J_i)/(J_e - J_{exp}) \quad (1)$$

These tautomerization constants can be calculated using representative δ_i/δ_e (or J_i/J_e) values for pure imine or enamine forms. The C-2 resonance has been considered in particular as this signal is very sensitive to the tautomerization process and experiences the most significant variations. Eqn (2) has been used in previous studies of Schiff bases derived from TRIS.[20,35]

$$K_T = (\delta_{C2} - 154.45)/(180.18 - \delta_{C2}) \quad (2)$$

The results obtained by application of such an equation to shifts taken from **25–28** are collected in Table 3. The population of imine molecules is approximately 50% for **25–27** at the equilibrium, whereas the enamine form slightly predominates in the case of **28**.

Computational calculations

Recently, Zhao and Truhlar[21] have recommended the use of the alternative functional, M06-2X, for main-group thermochemistry, barrier heights, and for the study of noncovalent interactions such as intramolecular hydrogen bonding. Bearing this premise in mind, gas-phase theoretical calculations of the energies at both the B3LYP/6-31G** and M06-2X/6-311++G** levels[36,37] with complete geometry optimization have been undertaken to ascertain the relative stability of imine and enamine structures and their propensity to interconvert. In addition, the role of the solvent effect has also been considered by using the SMD model[38] (DMSO as solvent, ε = 46.8). Further calculations of vibrational frequencies have also been performed in solution to estimate the tautomerization constants in terms of free energies. Selected geometrical parameters calculated for **25–28** in solution are collected in Table S5 (see ESI†).

Table 3 Relative energies[a] and tautomeric data in solution calculated for **25–28**

Comp.	Level	Imine	TS‡	Enamine	K_T	Imine (%)
25	B3LYP[b]	0.00	3.42	1.15		
	M06-2X[c]	0.00	5.03	2.99	0.88[f]	53[f]
	M06-2X[d]	0.00	3.93	1.13	0.01[g]	99[g]
	M06-2X[e]	0.00	2.99	2.84		
26	B3LYP[b]	0.00	3.27	1.10		
	M06-2X[c]	0.00	4.96	2.68	0.95[f]	51[f]
	M06-2X[d]	0.00	3.66	0.45	0.46[g]	68[g]
	M06-2X[e]	0.00	0.92	0.46		
27	B3LYP[b]	0.00	3.43	0.09		
	M06-2X[c]	0.00	5.13	2.20	0.97[f]	51[f]
	M06-2X[d]	0.00	4.05	0.23	0.47[g]	68[g]
	M06-2X[e]	0.00	1.79	0.44		
28	B3LYP[b]	0.00	3.27	0.12		
	M06-2X[c]	0.00	4.86	1.91	1.20[f]	45[f]
	M06-2X[d]	0.54	4.21	0.00	1.31[g]	43[g]
	M06-2X[e]	0.16	1.59	0.00		

[a] In kcal mol^{-1}. [b] At the B3LYP/6-31G** level in gas phase. [c] At the M06-2X/6-311++G** level in gas phase. [d] At the M06-2X/6-311++G** level, including the solvent effect (SMD model, DMSO as solvent). [e] Free energies at the M06-2X/6-311++G** level in DMSO. [f] Experimental data in solution (eqn (2)). [g] Calculated data from free energies at the M06-2X/6-311++G** level in DMSO.

The steric effect caused by two methyl groups at *ortho* positions in **26** and **28** is greater than that caused by the bulkier *tert*-butyl group in **25** and **27**. The effect manifests itself in larger dihedral angles C11–N1–C12–C13 (Tables S1–S4, see ESI†) for **26** and **28**.

The relative stabilities of optimized structures for both imine and enamine structures, as well as those of the corresponding transition states (Scheme 1) are summarized in Table 3, which reflect the greater stability of imine tautomers in the cases of **25** and **26** and approximately equal stability between the tautomers of **27** and **28**.

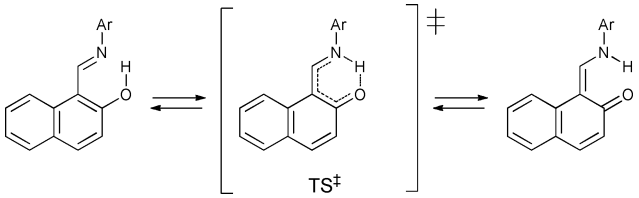

Scheme 1

As seen in Table 3, the use of the hybrid functional M06-2X//6-311++G** in gas-phase calculations predicts a greater stability of imine tautomers than the B3LYP functional does. At the M06-2X/6-311++G** level with inclusion of solvent effects, computation reveals that the imine form is scarcely stabilized in the cases of **25–27** though the opposite is observed for **28**. This matches relatively well the values obtained experimentally for K_T in solution for **26–28**, while for compound **25** the calculated molecular population of imine tautomer in solution is much higher than the experimental population obtained by using eqn (2) (Table 3).

Nevertheless, the low interconversion barrier (<5 kcal mol^{-1}) suggests a quick equilibrium at room temperature in the gas phase and in DMSO solution.

Since the interconversion between imine and enamine tautomers occurs intramolecularly, one can assume that the calculated energy for the transition states both in the gas phase (Fig. 3) and in solution (Table 3) will be roughly similar to that of the solid state.

Simulation of crystal packing

Experimental findings support the higher stability of imines in the solid state. Since there are no intermolecular interactions in the gas phase, the calculated stability represents the intrinsic stability of every tautomer. However, as previously pointed out,[39,40] the intermolecular interactions generated in the crystal lattice may invert the relative stability in the solid state. In solution, the relative stabilities can also be inverted by interaction with solvent molecules or by molecular aggregation.[39]

To simulate the packing effect and, on the basis of the crystal data obtained for **25**, we have incorporated into the calculation

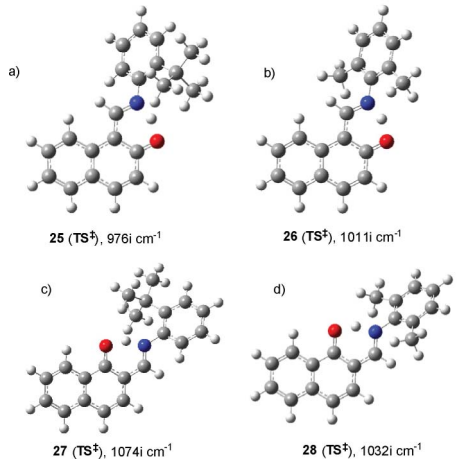

Fig. 3 Transition structures and their corresponding imaginary frequencies for imine-enamine interconversions in compounds **25–28** (at the M06-2X/6-311++G** level in the gas phase).

the five surrounding molecules possessing a close atom (as sum of van der Waals radii) to a central one (core molecule). This protocol gives rise to a whole system comprising 6 molecules and 264 atoms. The geometrical optimization at the B3LYP/6-31G** level has been carried out by fixing the X-ray parameters of the five surrounding molecules, and without any geometrical restriction for the core molecule. The resulting geometry for the six-molecule cluster with imine structures is collected in Fig. 4. Alternatively, the cluster incorporating five imine molecules around a central enamine tautomer is depicted in Fig. 5.

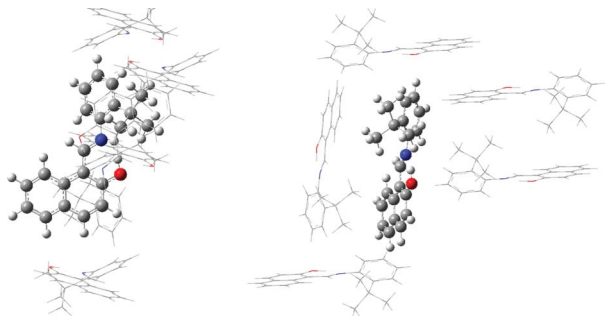

Fig. 4 Molecular cluster for compound **25** incorporating six molecules, all having an imine structure: frontal and side views (B3LYP/6-31G**).

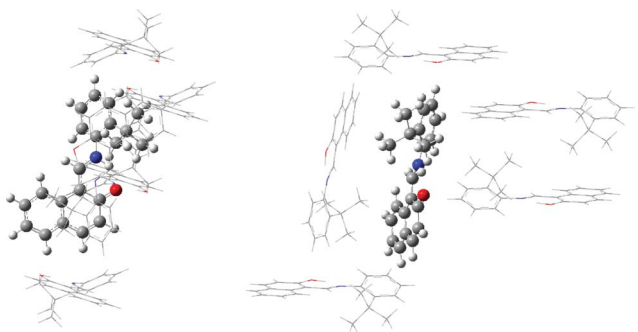

Fig. 5 Molecular cluster for compound **25** comprising five imine tautomers around an enamine form: frontal and side views (B3LYP/6-31G**).

The imine structure in the crystalline lattice (cluster) becomes more stable than the enamine one by 1.25 kcal mol^{-1}. The change in energy when the structure of one molecule of **25** in the gas phase is placed within the crystal can include two components: one is due to the change of the geometry, *i.e.* variations in bond lengths and angles (such a component will be destabilizing); and the other is due to the interaction involving the core molecule with the rest of the five surrounding ones.

The first component can be estimated by comparing the energy for isolated molecules in the gas phase with the energy associated with a geometry that results from removing the five surrounding molecules of the cluster. Such a comparison shows that one isolated imine is destabilized by 22.8 kcal mol^{-1} (591684.60–591661.79 kcal mol^{-1}), while the enamine form is destabilized by 21.6 kcal mol^{-1} (591683.45–591661.85 kcal mol^{-1}) at the B3LYP/6-31G** level. However, at the higher M06-2X/6-311++G** level of theory, such a destabilization becomes smaller (1.31 and 1.22 kcal mol^{-1} for imine and enamine, respectively). On the other hand, isolated imine and enamine structures of the cluster are coincidental in energy at the B3YP/6-31G** level. However, the imine tautomer is stabilized by 2.91 kcal mol^{-1} with respect to the enamine form at the M06-2X/6-311++G** level.

To calculate the interactions involving the core molecule with surrounding molecules in the cluster, the former must be removed. Such a calculation yielded an energy of –2957457.27 kcal mol^{-1} at the B3LYP/6-31G** level. The sum of the latter plus the energy of the isolated imine or enamine core in the cluster (–3549119.06 and –3549119.12 kcal mol^{-1}, respectively) were then compared with the global energies obtained for the clusters with imine and enamine structures (Table 4). Such a comparison shows how the interaction of peripheral molecules with the core one in the packing stabilizes the imine tautomer by 152.16 kcal mol^{-1} (3549271.22–3549119.06 kcal mol^{-1}), while the enamine-based cluster is stabilized by 150.85 kcal mol^{-1} (3549269.97–3549119.12 kcal mol^{-1}). Overall, a core molecule possessing an imine structure becomes more stabilized than its enamine tautomer by 1.31 kcal mol^{-1}.

Conclusions

The structures of Schiff bases **25–28**, generated by condensation of 2-hydroxy-1-naphthaldehyde, or 1-hydroxy-2-naphthaldehyde, with *o*-substituted anilines have been elucidated in the solid state by both IR spectroscopy and low-temperature X-ray diffraction, and in solution through NMR analysis. Solid-state structures are consistent with imine tautomers, although electron density difference maps point to some delocalization of the hydrogen atom between oxygen and nitrogen atoms, especially in compounds **27** and **28**. In solution such bases exhibit rapid equilibria, which are slightly shifted to the imine tautomer in the cases of **25–27** as inferred from an estimation of their tautomerization constants. DFT calculations employing two hybrid functionals (the standard B3LYP/6-31G** and the higher M06-2X/6-311++G**) also corroborate the above findings. Finally, in an attempt to shed light into the preferential occurrence of imine structures in the solid state, the crystal lattice of **25** has been simulated and computed at the B3LYP/6-31G** level. This high-cost computational study takes into account the interaction of an imine or enamine core molecule with a first sphere of five imine molecules as emerge from crystal data. By comparing this cluster effect with the stability of

Table 4 Calculated total and relative energies (in parenthesis) (kcal mol^{-1}) for imine-enamine tautomers of compound **25**

Structure		Imine	Enamine
Isolated	Gas phase[a]	−591684.60 (0.00)	−591683.45 (1.15)
	Core geometry[a]	−591661.79 (22.81)	−591661.85 (22.75)
	Gas phase[b]	−591563.41 (0.00)	−591560.41 (3.00)
	Core geometry[b]	−591562.10 (1.31)	−591559.19 (4.22)
Associated	Cluster[a]	−3549271.22 (0.00)	−3549269.97 (1.25)
Pheripheral plus core geometry[a]		−3549119.06 (152.16)	−3549119.12 (152.10)

[a] At the B3LYP/6-31G** level. [b] At the M06-2X/6-311++G** level.

isolated molecules, the greater stabilization of an imine tautomer (about 1.3 kcal mol^{-1} relative to its enamine counterpart) is shown to reflect the differences in molecular packing.

Experimental

Materials and methods

All the chemicals and solvents were of analytical grade and used as received. 2-*tert*-butylaniline, 2,6-dimethylaniline, and 2-hydroxy-1-naphthaldehyde were purchased from Aldrich Chemical Co. Inc. and 1-hydroxy-2-naphthaldehyde from TCI-Europe, and used without any further purification. FT-IR spectra were recorded in the range of 4000–600 cm^{-1} on a THERMO spectrophotometer. Solid samples were recorded on KBr (Merck) pellets. NMR spectra were recorded on Bruker 400/500 AC/PC instruments. Assignments were confirmed by homo- and hetero-nuclear double-resonance and DEPT (distortionless enhancement by polarization transfer). TMS was used as the internal standard (δ = 0.00 ppm) and all J values are given in Hz. Microanalyses were determined on a Leco 932 analyzer.

X-Ray data collection and structural refinement

Cell dimensions and intensity data for **25–28** were recorded at 120 K, using a Bruker Nonius KappaCCD area detector diffractometer mounted at the window of a rotating Mo anode (λ(Mo-Kα) = 0.71073 Å). Data collection and processing were carried out using the programs COLLECT[41] and DENZO[42] and an empirical absorption correction was applied using SADABS[43]

The structures were solved *via* direct methods[44] and refined by full matrix least squares on F^2. Maximum, minimum peaks (e Å^{-3}) in the final difference Fourier synthesis were found as 0.20, –0.25 (**25**); 0.16, –0.21 (**26**); 0.20, –0.27 (**27**), and 0.19, –0.20 (**28**), respectively. The hydrogen atoms in both structures were placed in calculated positions and included in the refinement using a riding model approximation. The hydroxyl hydrogens atoms were first located in the difference map and then included in the refinement using a riding model, the torsion angle was allowed to refine and in all cases matched the position identified in the difference map. Crystallographic illustrations were prepared using the CAMERON programs.[45] The molecular structures with the atom-numbering scheme are shown in Fig. 1.[23] All the relevant crystallographic data and structure refinement parameters for **25–28** are summarized in Table S6 (see ESI†). Selected bond distances and angles are listed in Tables S1–S4 (see ESI†). Inter- and intramolecular hydrogen bond data [Å and °] for compounds **25–28** are listed in Table 1.

Computational details

Theoretical calculations were carried out using the Gaussian09 package.[46] The B3LYP/6-31G** and M06-2X/6-311++G** density-functional methods[36,37] were selected for all the geometry optimizations and frequency analysis.

General procedure for the synthesis of Schiff bases

To a solution of the aniline derivative (2.90 mmol) in ethanol (10 mL) was slowly added a solution of the corresponding aldehyde (2.90 mmol) in a small volume of methanol (~5 mL). When the title compound did not precipitate, the mixture was evaporated under vacuum and gave rise to a solid on standing or on cooling. The resulting product was collected by filtration, washed successively with cold water, ethanol, and diethyl ether, and recrystallized from ethanol or methanol.

1-*tert*-Butyl-2-(2-hydroxy-1-naphthylmethylene)aminobenzene (25)

From 2-hydroxy-1-naphtaldehyde and 2-*tert*-butylaniline: (0.774 g, 88%), m.p. 103–105 °C, IR (ν, KBr): 1622 (CH═N), 1602, 1578, 1561, 1481 cm^{-1} (arom). ^{1}H NMR (400 MHz, DMSO-d_6): δ 15.34 (1H, s, OH), 9.46 (1H, s, CH═N), 8.51 (1H, d, J = 8.8 Hz, H-arom), 8.00 (1H, d, J = 9.2 Hz, H-arom), 7.85 (1H, d, J = 7.6 Hz, H-arom), 7.55 (1H, t, J = 8.0 Hz, H-arom), 7.45 (1H, d, J = 7.6 Hz, H-arom), 7.35 (4H, m, H-arom), 7.15 (1H, d, J = 9.2 Hz, H-arom), 1.43 (9H, s, CH_3). ^{13}C NMR (100 MHz, DMSO-d_6): δ 166.5 (C-OH), 159.0 (C═N), 146.7, 142.3, 136.6, 133.3, 129.5, 128.6, 128.1, 127.5, 127.0, 126.7, 124.0, 122.9, 121.1, 121.0, 109.8 (C-arom), 35.3, 31.0 (C[CH_3]$_3$). Analysis calcd. for $C_{21}H_{21}NO$ (303.40): C, 83.13; H, 6.98; N, 4.62. Found: C, 83.01; H, 6.92; N, 4.78.

2-(2-Hydroxy-1-naphthylmethylene)amino-1,3-dimethylbenzene (26)

From 2-hydroxy-1-naphtaldehyde and 2,6-dimethylaniline: (0.639 g, 80%), m.p. 117–119 °C, IR (ν, KBr): 1622 (CH═N), 1606, 1572, 1469 cm^{-1} (arom). ^{1}H NMR (400 MHz, DMSO-d_6): δ 15.29 (1H, d, J = 2.4 Hz, OH), 9.44 (1H, d, J = 2.4 Hz, CH═N), 8.38 (1H, d, J = 8.8 Hz, H-arom), 7.98 (1H, d, J = 9.2 Hz, H-arom), 7.84 (1H, d, J = 8.0 Hz, H-arom), 7.50 (1H, m, H-arom), 7.36 (1H, t, J = 7.6 Hz, H-arom), 7.11 (4H, m, H-arom), 2.24 (6H, s, CH_3). ^{13}C NMR (100 MHz, DMSO-d_6): δ 167.0 (C-OH), 163.5 (CH═N), 145.9, 136.3, 133.4, 129.6, 129.4, 128.9, 128.6, 127.4, 125.8, 123.9, 121.3, 120.7, 108.9 (C-arom), 18.7 (CH_3). Analysis calcd. for $C_{19}H_{17}NO$

(275.34): C, 82.88; H, 6.22; N, 5.09. Found: C, 82.68; H, 6.09; N, 5.17.

1-*tert*-Butyl-2-(1-hydroxy-2-naphthylmethylene)aminobenzene (27)

From 1-hydroxy-2-naphtaldehyde and 2-*tert*-butylaniline: (0.721 g, 82%), m.p. 127-129 °C, IR (ν, KBr): 1603 (CH═N), 1156, 1478 cm^{-1} (arom). ^1H NMR (500 MHz, DMSO-d_6): δ 14.78 (1H, d, J = 3.5 Hz, OH), 8.77 (1H, d, J = 3.5 Hz, CH═N), 8.35 (1H, d, J = 8.0 Hz, H-arom), 7.81 (1H, d, J = 8.0 Hz, H-arom), 7.64 (1H, t, J = 7.5 Hz, H-arom), 7.52 (2H, m, H-arom), 7.45 (1H, d, J = 8.0 Hz, H-arom), 7.33 (3H, m, H-arom), 7.22 (1H, t, J = 8.5 Hz, H-arom), 1.46 (9H, s, CH_3). ^{13}C NMR (125 MHz, DMSO-d_6): δ 167.1 (C-OH), 161.4 (C═N), 144.9, 142.0, 136.9, 130.3, 128.9, 128.1, 128.0, 127.1, 126.9, 126.9, 126.0, 124.5, 122.2, 117.3, 112.2 (C-arom), 35.2, 30.9 (C[CH_3]$_3$). Analysis calcd. for $C_{21}H_{21}NO$ (303.40): C, 83.13; H, 6.98; N, 4.62. Found: C, 83.25; H, 6.73; N, 4.63.

2-(1-Hydroxy-2-naphthylmethylene)amino-1,3-dimethylbenzene (28)

From 1-hydroxy-2-naphtaldehyde and 2,6-dimethylaniline: (0.575 g, 72%), m.p. 115–117 °C, IR (ν, KBr): 1607 (CH═N), 1588, 1562, 1503, 1467 cm^{-1} (arom). ^1H NMR (400 MHz, DMSO-d_6): δ 14.67 (1H, d, J = 4.4 Hz, OH), 8.61 (1H, d, J = 4.4 Hz, CH═N), 8.34 (1H, d, J = 8.0 Hz, H-arom), 7.80 (1H, d, J = 8.0 Hz, H-arom), 7.64 (1H, t, J = 7.6 Hz, H-arom), 7.52 (1H, t, J = 7.6 Hz, H-arom), 7.43 (1H, d, J = 8.8 Hz, H-arom), 7.13 (4H, m, H-arom), 2.27 (6H, s, CH_3). ^{13}C NMR (100 MHz, DMSO-d_6): δ 168.5 (C-OH), 165.5 (C═N), 143.7, 136.9, 130.3, 130.2, 129.0, 128.8, 128.0, 127.4, 126.3, 125.9, 124.5, 116.7, 111.1 (C-arom), 18.7 (CH_3). Analysis calcd. for $C_{19}H_{17}NO$ (275.34): C, 82.88; H, 6.22; N, 5.09. Found: C, 83.09; H, 6.32; N, 5.25.

Acknowledgements

This work was supported by the *Junta de Extremadura* (PRI08A032) and the *Ministerio de Educación y Ciencia* and *FEDER* (CTQ2010-18938/BQU). The Research & Technological Innovation and Supercomputing Center of Extremadura (CénitS) is gratefully acknowledged for permitting the use of the supercomputer LUSITANIA.

Notes and references

1 (*a*) M. Guillaume, B. Champagne, N. Markova, V. Enchev and F. Castet, *J. Phys. Chem. A*, 2007, **111**, 9914; (*b*) J. Harada, T. Fujiwara and K. Ogawa, *J. Am. Chem. Soc.*, 2007, **129**, 16216; (*c*) P. Przybylsky, A. Huczynski, K. Pyta, B. Brzezinski and F. Bartl, *Curr. Org. Chem.*, 2009, **13**, 124.
2 (*a*) P. I. Nagy and W. M. F. Fabian, *J. Phys. Chem. B*, 2006, **110**, 25026; (*b*) A. Filarowski, A. Koll and L. Sobczyk, *Curr. Org. Chem.*, 2009, **13**, 172.
3 W. Rodríguez-Córdoba, J. S. Zugazagoitia, E. Collado-Fregoso and J. Peon, *J. Phys. Chem. A*, 2007, **111**, 6241.
4 P. Gilli, V. Bertolasi, L Pretto, A. Lyčka and G. Gilli, *J. Am. Chem. Soc.*, 2002, **124**, 13554.
5 (*a*) G. Pavlovic and J. M. Sosa, *Acta Crystallogr., Sect. C: Cryst. Struct. Commun.*, 2000, **56**, 1117; (*b*) S. Yüce, A. Ozëk, Ç. Albayrak, M. Odabasoglu and O. Büyükgüngör, *Acta Crystallogr., Sect. E: Struct. Rep. Online*, 2004, **60**, o1217; (*c*) A. Ozëk, S. Yüce, Ç. Albayrak, M. Odabasoglu and O. Büyükgüngör, *Acta Crystallogr., Sect. E: Struct. Rep. Online*, 2004, **60**, o826; (*d*) M. Odabasoglu, Ç. Albayrak and O. Büyükgüngör, *Acta Crystallogr., Sect. E: Struct. Rep. Online*, 2003, **60**, o142; (*e*) I. Dilovic, D. Matkovic-Calogovic, Z. Popovic and V. Roje, *Acta Crystallogr., Sect. C: Cryst. Struct. Commun.*, 2005, **61**, m351; (*f*) A. Ozëk, S. Yüce, Ç. Albayrak, M. Odabasoglu and O. Büyükgüngör, *Acta Crystallogr., Sect. E: Struct. Rep. Online*, 2004, **60**, o1162; (*g*) *ibid*, 828.
6 E. Acevedo-Aranz, J. M. Fernández-G, M. J. Rosales-Hoz and R. A. Toscano, *Acta Crystallogr., Sect. C: Cryst. Struct. Commun.*, 1992, **48**, 115.
7 Y. Elerman, M. Kabak, A. Elmali and I. Svoboda, *Acta Crystallogr., Sect. C: Cryst. Struct. Commun.*, 1998, **54**, 128.
8 A. Ozëk, S. Yüce, Ç. Albayrak, M. Odabasoglu and O. Büyükgüngör, *Acta Crystallogr., Sect. E: Struct. Rep. Online*, 2004, **60**, o356.
9 T. Hökelek, N. Gündük, Z. Hayvali and Z. Kilic, *Acta Crystallogr., Sect. C: Cryst. Struct. Commun.*, 1995, **51**, 880.
10 B. Kaitner and G. Pavlovic, *Acta Crystallogr., Sect. C: Cryst. Struct. Commun.*, 1996, **52**, 2573.
11 Z. Popovic, V. Roje, G. Pavlovic, D. Matkovic-Calogovic and G. Giester, *J. Mol. Struct.*, 2001, **597**, 39.
12 H. Nazir, M. Yildiz, H. Yilmaz, M. N. Tahir and D. Ülkü, *J. Mol. Struct.*, 2000, **524**, 241.
13 S. Gao, L.-H. Huo, H. Zhao and S. W. Ng, *Acta Crystallogr., Sect. E: Struct. Rep. Online*, 2004, **61**, 192.
14 C.-L. Yuan, *Acta Crystallogr., Sect. E: Struct. Rep. Online*, 2005, **61**, o1182.
15 H.-L. Zhu and Z.-L. You, *Acta Crystallogr., Sect. E: Struct. Rep. Online*, 2005, **61**, o1271.
16 P. M. Dominiak, E. Grech, G. Barr, S. Teat, P. Mallinson and K. Woźniak, *Chem.–Eur. J.*, 2003, **9**, 963.
17 G. Pavolic, J. M. Sosa, D. Vikic-Topic and I. Leban, *Acta Crystallogr., Sect. B: Struct. Sci.*, 2002, **58**, 317.
18 A. J. Gallant, M. Yun, M. Sauer, C. S. Yeung and M. J. MacLachlan, *Org. Lett.*, 2005, **7**, 4827.
19 (*a*) R. F. Martínez, M. Ávalos, R. Babiano, P. Cintas, J. L. Jiménez, M. E. Light, J. C. Palacios and E. M. S. Pérez, *Eur. J. Org. Chem.*, 2010, 5263; (*b*) *ibid*, 6224.
20 R. F. Martínez, M. Ávalos, R. Babiano, P. Cintas, J. L. Jiménez, M. E. Light and J. C. Palacios, *Eur. J. Org. Chem.*, 2011, 3137.
21 Y. Zhao and D. G. Truhlar, *Acc. Chem. Res.*, 2008, **41**, 157.
22 (*a*) L. J. Bellamy, in *The Infrared Spectra of Complex Molecules*, vol I, 3rd ed. Chapman and Hall, London, 1975, pp 299-305; (*b*) E. Pretsch, P. Bühlmann, C. Alffolter, A. Herrera and R. Martínez, in *Determinación estructural de compuestos orgánicos*, Springer-Verlag Ibérica, Barcelona, 2001, pp 273 and 286.
23 Crystal data of structures reported in this work have been deposited with the Cambridge Crystallographic Data Centre with numbers CCDC-805572 (**25**), CCDC-805573 (**26**), CCDC- 810937 (**27**), and CCDC-805574 (**28**); they can be obtained free of charge *via* www.ccdc.cam.ac.uk/data_request/cif.
24 M. Odabaşoğlu, Ç. Albayrak, R. Özkanza, F. Z. Aykan and P. Lonecke, *J. Mol. Struct.*, 2007, **840**, 71.
25 A. Karakaş, A. Elmali, H. Ünver and I. Svoboda, *J. Mol. Struct.*, 2004, **702**, 103.
26 W. Schilf, B. Kamieński, B. Kolodziej and E. Grech, *J. Mol. Struct.*, 2004, **708**, 33.
27 (*a*) B. Kamieński, W. Schilf, T. Dziembowska, Z. Rozwadoski and A. Szady-Chelmieniecka, *Solid State Nucl. Magn. Reson.*, 2000, **16**, 285; (*b*) W. Schilf, B. Kamieński, T. Dziembowska, Z. Rozwadoski and A. Szady-Chelmieniecka, *J. Mol. Struct.*, 2000, **552**, 33.
28 S. Berger, S. Braun and H.-O. Kalinowski, in *NMR Spectroscopy of the Non-Metallic Elements*, Wiley, Chichester, 1996.
29 S. H. Alarcón, A. C. Olivieri, D. Sanz, R. M. Claramunt and J. Elguero, *J. Mol. Struct.*, 2004, **705**, 1.
30 W. Schilf, J. P. Bloxsidge, J. R. Jones and S.-Y. Lu, *Magn. Reson. Chem.*, 2004, **42**, 556.
31 W. Schilf, B. Kamieński, A. Szady-Chelmieniecka and E. Grech, *J. Mol. Struct.*, 2005, **743**, 237.
32 W. Schilf, B. Kamieński, A. Szady-Chelmieniecka, E. Grech, A. Makal and K. Woźniak, *J. Mol. Struct.*, 2007, **844–845**, 94.
33 (*a*) G. O. Dudek and E. P. Dudek, *J. Am. Chem. Soc.*, 1964, **86**, 4283; (*b*) G. O. Dudek and E. P. Dudek, *Chem. Commun.*, 1965, 464; (*c*) G. O. Dudek and E. P. Dudek, *J. Am. Chem. Soc.*, 1966, **88**, 2407.

34 W. Schilf, *J. Mol. Struct.*, 2004, **689**, 245.
35 This equation is similar to that of Alarcón *et.al.*[29] $\delta_i$and $\delta_e$were taken as the lowest and the highest δ_{C2}shift measured experimentally for a series of Schiff bases derived from TRIS. The, former corresponds to the δ_{C2}resonance obtained for the 5-hydroxysalicyl derivative, while δ_e was measured in the 5-nitrosalicyl derivative: R. F. Martínez, Ph.D. Thesis, Universidad de Extremadura, 2010.
36 Y. Zhao and D. G. Truhlar, *Theor. Chem. Acc.*, 2007, **120**, 215.
37 (*a*) A. D. Becke, *J. Chem. Phys.*, 1993, **98**, 5648; (*b*) C. Lee, W. Yang and R. G. Parr, *Phys. Rev. B*, 1988, **37**, 785.
38 A. V. Marenich, C. J. Cramer and D. G. Truhlar, *J. Phys. Chem. B*, 2009, **113**, 6378.
39 K. Ogawa and J. Harada, *J. Mol. Struct.*, 2003, **647**, 211.
40 K. Ogawa, Y. Kasahara, Y. Ohtani and J. Harada, *J. Am. Chem. Soc.*, 1998, **120**, 7107.
41 R. Hooft and B. V. Nonius, *COLLECT: Data Collection Software*, Nonius BV, The Netherlands, 1998.
42 Z. Otwinowski and W. Minor *Macromolecular Crystallography, part A*C. W. Carter Jr., R. M. Sweet, ed. *Methods in Enzymology*, 1997, **276**, 307Academic Press, San Diego, CA.
43 G. M. Sheldrick, *SADABS-Bruker Nonius Area Detector Scaling and Absorption Correction-v2.10*, 1993.
44 G. M. Sheldrick, *SHELX97: Programs for Crystal Structure Analysis (Release 97-2)*Institüt für Anorganische Chemie der Universität, Tammanstrasse 4, D-3400, Göttingen, Germany, 1998.
45 D. M. Watkin, L. Pearce and C. K. Prout, *CAMERON. A Molecular Graphics Package*; Chemical Crystallography Laboratory, University of Oxford, England, 1993.
46 *Gaussian 09, Revision B.01*, M. J. Frisch, G. W. Trucks, H. B. Schlegel, G. E. Scuseria, M. A. Robb, J. R. Cheeseman, G. Scalmani, V. Barone, B. Mennucci, G. A. Petersson, H. Nakatsuji, M. Caricato, X. Li, H. P. Hratchian, A. F. Izmaylov, J. Bloino, G. Zheng, J. L. Sonnenberg, M. Hada, M. Ehara, K. Toyota, R. Fukuda, J. Hasegawa, M. Ishida, T. Nakajima, Y. Honda, O. Kitao, H. Nakai, T. Vreven, J. A. Montgomery, Jr., J. E. Peralta, F. Ogliaro, M. Bearpark, J. J. Heyd, E. Brothers, K. N. Kudin, V. N. Staroverov, R. Kobayashi, J. Normand, K. Raghavachari, A. Rendell, J. C. Burant, S. S. Iyengar, J. Tomasi, M. Cossi, N. Rega, J. M. Millam, M. Klene, J. E. Knox, J. B. Cross, V. Bakken, C. Adamo, J. Jaramillo, R. Gomperts, R. E. Stratmann, O. Yazyev, A. J. Austin, R. Cammi, C. Pomelli, J. W. Ochterski, R. L. Martin, K. Morokuma, V. G. Zakrzewski, G. A. Voth, P. Salvador, J. J. Dannenberg, S. Dapprich, A. D. Daniels, Ö. Farkas, J. B. Foresman, J. V. Ortiz, J. Cioslowski and D. J. Fox, Gaussian, Inc., Wallingford CT, 2010.